

## Nonresonant coherent control: Intersubband excitations manipulated by a nonresonant terahertz pulse

Giulia Folpini,<sup>1</sup> Drew Morrill,<sup>1</sup> Carmine Somma,<sup>1</sup> Klaus Reimann,<sup>1,\*</sup> Michael Woerner,<sup>1,†</sup> Thomas Elsaesser,<sup>1</sup> and Klaus Biermann<sup>2</sup>

<sup>1</sup>Max-Born-Institut für Nichtlineare Optik und Kurzzeitspektroskopie, 12489 Berlin, Germany

<sup>2</sup>Paul-Drude-Institut für Festkörperelektronik, 10117 Berlin, Germany

(Received 23 January 2015; revised manuscript received 22 July 2015; published 17 August 2015)

We present an approach for controlling quantum coherences in condensed matter by interaction with a nonresonant optical control field. Coherent intersubband (IS) excitations of electrons in GaAs/AlGaAs quantum wells are manipulated by a strong nonresonant terahertz (THz) field as demonstrated by phase-resolved two-color two-dimensional spectroscopy. In the linear regime of IS response, we observe a THz-induced enhancement of the midinfrared (MIR) IS absorption and a dispersive perturbed free induction decay caused by a THz-induced blueshift of the IS polarization. In the regime of IS Rabi oscillations, the THz field causes pronounced phase shifts of the coherently emitted MIR field, while the IS Rabi frequency remains unaffected. Such behavior is accounted for by a full solution of the Maxwell-Bloch equations, treating the THz and MIR fields without approximations. Our control scheme paves the way for THz control of IS emitters and holds potential for an extension to other systems.

DOI: [10.1103/PhysRevB.92.085306](https://doi.org/10.1103/PhysRevB.92.085306)

PACS number(s): 78.67.De, 42.50.Md, 73.21.Fg, 78.47.jh

### I. INTRODUCTION

Quantum coherences induced by optical excitation have developed into a vibrant research area of condensed matter physics. In the most elementary approach, resonant interaction of a light field with a transition dipole locks the quantum phases of the optically coupled states and induces a coherent macroscopic polarization of matter. Within a time interval limited by the dephasing time, this polarization can be manipulated by repetitive interactions with the light field, allowing for “coherent control” of the material’s excitation [1,2]. In condensed matter systems, decoherence of optical polarizations typically occurs on ultrafast time scales and limits the time range accessible for coherent control to a few picoseconds at most.

The controlled shaping of optical pulses in the femtosecond time domain has led to demonstrations of coherent control in a large variety of systems. In first experiments, a pair of phase-locked pulses interacting resonantly with the medium was used to coherently control charge oscillations and excitonic polarizations [3–5]. More sophisticated schemes of exciting one- and two-photon transitions phase coherently [6] or spatiotemporal coherent control of photoelectron emission on a subwavelength scale [7] or of phonons [8] have widened the range of applications. In photochemistry, control of the outcome of photoreactions has first been demonstrated in the gas phase [9,10], followed by work on steering molecular dynamics in the liquid phase [11,12]. Here, adaptive learning algorithms [10,13] have been applied for optimizing the yield of particular species generated by the photochemical reaction. The concept of adiabatic passage introduces typically pulses of more than one color in the experiment and exploits also slightly off-resonant light-matter interactions [14,15].

So far, nearly all experimental schemes for coherent control have concentrated on a manipulation of the system

under conditions of resonant excitation, i.e., a sequence of pulses interacts with single- and/or multiphoton resonances. In contrast, the application of distinctly off-resonant electric field transients for controlling resonant optical excitations has remained scarce [16]. The latter scheme requires a high amplitude of the off-resonant field with frequency  $\nu$  to make the interaction energy with the system comparable to the transition energy of the optical resonance. According to the dressed-state picture developed by Autler and Townes [17,18], one has to consider not just the electronic states alone, but combined states of electron and light, e.g., the state consisting of the electron in level 1 and one photon with energy  $h\nu$ ,  $|n = 1, 1h\nu\rangle$  [Fig. 1(a)]. Because of the interaction with the electric field, the states  $|n = 1, 1h\nu\rangle$  and  $|n = 2, 0h\nu\rangle$  repel each other [arrows in Fig. 1(a)], leading to a blueshift of the transition frequency for  $\nu < \nu_0$  and to a redshift for  $\nu > \nu_0$  ( $\nu_0$  is the unperturbed transition frequency between states  $n = 1$  and  $n = 2$ ). The magnitude of the shift is proportional to  $(d_0 E)^2$ , with  $d_0$  the electric dipole moment for the transition and  $E$  the amplitude of the off-resonant electric field.

While the Autler-Townes treatment focuses on the *time-averaged* behavior of a two-level system in an external off-resonant field, off-resonant control requires insight into the *dynamics* of coherent interactions. Here, techniques of field-resolved detection of optical transients hold particularly strong potential for mapping the system’s response in amplitude and phase. In this work, we demonstrate and analyze a scheme for coherently controlling resonant optical excitations by strong off-resonant electric fields in the THz frequency range. As a model system, we study optical transitions between different confined subbands in low-dimensional semiconductors which are fundamental elementary excitations of free electrons [19]. Such intersubband (IS) excitations represent sensitive probes of the complex many-body and scattering behavior of electrons and have been studied by both experiment and theory [20–24]. Moreover, optoelectronic devices such as quantum cascade lasers [25–27] and infrared detectors [28] rely on IS transitions.

\*reimann@mbi-berlin.de

†woerner@mbi-berlin.de

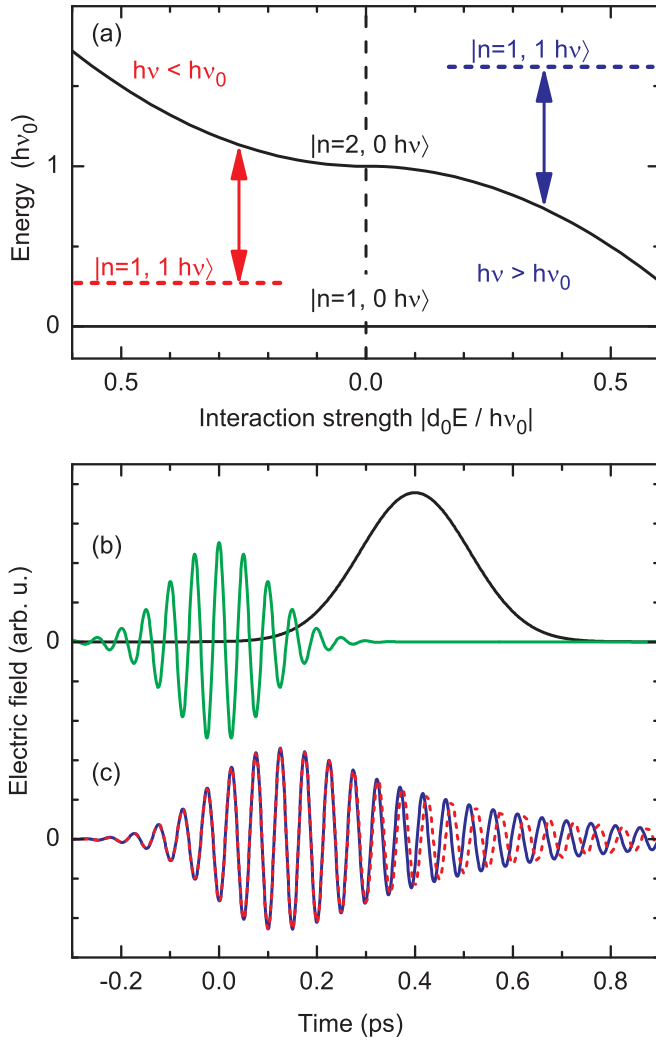


FIG. 1. (Color online) (a) Energies of a two-level system exposed to a strong nonresonant driving field  $E$  as a function of the normalized interaction energy  $|d_0 E / h\nu_0|$ , on the left for  $\nu < \nu_0$  and on the right for  $\nu > \nu_0$ . In the dressed-state picture the repulsion (arrows) of the state  $|n=2, 0h\nu\rangle$  from the state  $|n=1, 1h\nu\rangle$  leads for  $\nu < \nu_0$  to a blueshift and for  $\nu > \nu_0$  to a redshift of the optical transition. (b),(c) Sequential coherent control of both amplitude and phase of the excitation of a two-level system. (b) Electric field transients of a resonant (green) and of a nonresonant THz pulse (black). (c) Interaction with the resonant pulse creates a coherent polarization emitting an electric field (red dashed line). The interaction with the THz pulse introduces a phase shift of the emitted field (blue solid line).

Dynamics of IS excitations are inherently ultrafast with decoherence times of several hundreds of femtoseconds [29] and picosecond population lifetimes of electrons in higher subbands. Nevertheless, IS Rabi oscillations [30] have been induced by resonant femtosecond electric field transients and read out using the field radiated from the coherent IS polarization [23]. In our present study, the nonresonant THz field manipulates linear and nonlinear IS polarizations. The THz field induces well-defined phase shifts in the coherent IS emission while the IS Rabi frequency, a measure of the coupling between the IS dipole and the midinfrared

(MIR) field, remains unaffected by the control field. The data are analyzed within the framework of a dressed state picture accounting for the experimental results. Apart from its fundamental relevance for the nonlinear IS response, this two-color scenario is of high interest for all-optical control.

## II. EXPERIMENT

### A. Sample geometry

The sample was grown by molecular beam epitaxy on an insulating GaAs substrate. It contains 20 GaAs QWs of  $L = 11$  nm width, separated by 20 nm wide  $\text{Al}_{0.35}\text{Ga}_{0.65}\text{As}$  barriers. The barriers are  $\delta$  doped to achieve an electron concentration of  $5 \times 10^{11} \text{ cm}^{-2}$  per QW. As the thickness of the QW stack is small compared to both THz and MIR wavelengths, all QWs experience a similar electric field [31]. The  $1 \rightarrow 2$  IS absorption [solid line in Fig. 2(d)] has a frequency of  $\nu_0 = 21$  THz. The observed width of 2.4 THz is limited by the spectral resolution of the spectrometer used. To achieve sufficient coupling between the MIR field and the IS transition dipole oriented along the growth direction  $z$ , the sample is polished as a  $90^\circ$  prism [32,33]. Half of the bottom surface of the prism is gold coated to generate a standing wave [34] with a total field in  $z$  direction [Fig. 2(b)], for total reflection from the uncoated prism bottom [Fig. 2(c)], the

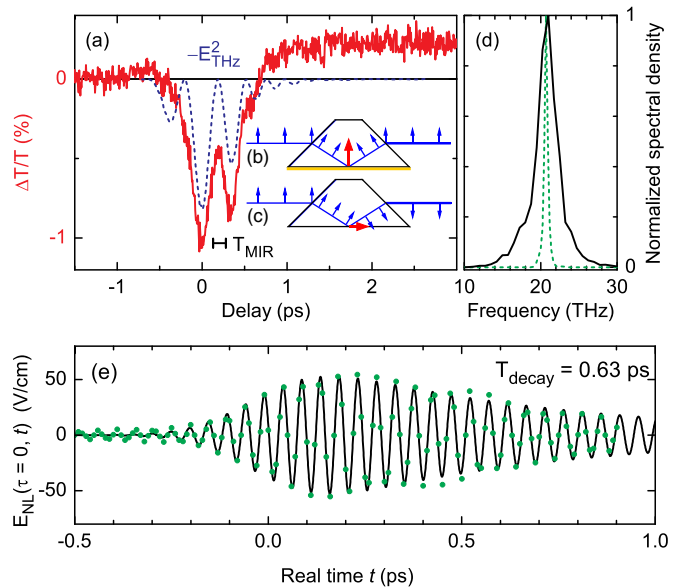


FIG. 2. (Color online) (a) Solid line, THz-induced change of the time-integrated MIR transmission through the sample with gold coating as a function of delay. Also shown (dashed line) is the square of the THz electric field (normalized, the maximum amplitude is 30 kV/cm) and the width  $T_{\text{MIR}}$  of the MIR pulse (amplitude 3 kV/cm). Direction of the electric field at the quantum wells (b) with gold coating (metallic reflection, amplitude reflection  $r = +1$ ) and (c) without coating (total reflection,  $r = -1$ ). IS transitions are only allowed in case (b). (d) IS absorption of the sample (black solid line) and Fourier transform (dashed line) of the perturbed free-induction decay (PFID) measured at  $\tau = 0$  for low MIR amplitude [dots in (e)]. (e) Measured PFID (green dots) and fit (black line) giving a polarization decay time of  $T_{\text{decay}} = 0.63$  ps.

$z$  component of the total field and thus the interaction with the IS dipoles vanishes.

### B. Time-resolved experiments

Synchronized THz and MIR pulses are generated with a Ti:sapphire oscillator-amplifier system by difference frequency mixing. The spectrum of the THz pulses has a FWHM of 0.9 THz and a center frequency of 1.2 THz, nonresonant to the IS transition. The peak amplitude of the THz pulses is 30 kV/cm. The MIR pulses of 150 fs duration have amplitudes between 3 and 100 kV/cm. The MIR pulses are centered at the IS transition frequency and have a spectral width of 6 THz (FWHM). Both MIR and THz pulses are focused onto the sample kept at a temperature of 30 K.

In a first series of THz-pump–MIR-probe measurements, changes in the MIR transmission through the sample are measured as a function of the delay between the THz and MIR pulses using a time-integrating HgCdTe detector. The transient presented in Fig. 2(a) shows the change of MIR transmission  $\Delta T/T_0 = (T - T_0)/T_0$  as a function of pump-probe delay ( $T$ ,  $T_0$ : sample transmission with and without THz pump). For a low MIR electric field amplitude of 3 kV/cm, we observe a transmission decrease during the temporal pulse overlap, followed by a transmission increase, which decays with a time constant of 1 ns [35–37]. The signal during pulse overlap is proportional to the square of the THz electric field (dashed line), convoluted with the finite width of the MIR pulse. For higher MIR amplitudes, this signal *decreases*, while the time evolution of  $\Delta T/T_0$  remains unchanged.

For a more detailed insight, we implemented two-color 2D spectroscopy by measuring the THz and MIR fields transmitted through the sample as a function of both  $\tau$ , the delay between the two pulses, and the real time  $t$ . A phase-resolved detection scheme based on electrooptic sampling [38,39] included a 10  $\mu\text{m}$  thick (110) ZnTe crystal and 13 fs probe pulses from the oscillator of the Ti:sapphire laser system. Using choppers synchronized to the amplifier repetition rate, we created three different pulse sequences: THz pulse alone, MIR pulse alone, and both pulses together [40,41].

In a first set of phase-resolved measurements, we determined the nonlinear IS response in the MIR by detecting the emitted field  $E_{\text{em}}(t)$  without applying a THz field. To separate the IS response from other effects such as reflections at the prism surfaces or dispersion in the substrate, we measure the transmitted electric field at a position with gold coating [ $E_{\text{tr}}^{\text{gold}}(t)$ ] and at a position without [ $E_{\text{tr}}^{\text{no}}(t)$ ]. Since the IS response contributes only to  $E_{\text{tr}}^{\text{gold}}(t)$ , the sum  $E_{\text{em}}(t) = E_{\text{tr}}^{\text{gold}}(t) + E_{\text{tr}}^{\text{no}}(t)$  gives the field emitted by the IS polarization [42].

The field responsible for exciting the IS polarization is the local electric MIR field  $E_{\text{lo}}(t)$  acting on the QWs, i.e., the field component normal to the QWs. The prism geometry with a gold coating used here [Fig. 2(b); see also Fig. 3(b) of Ref. [24]] leads to an enhanced local field  $E_{\text{lo}}(t) = \alpha[E_{\text{tr}}^{\text{gold}}(t) - E_{\text{tr}}^{\text{no}}(t)]$  because of the constructive interference with the waves reflected off the gold mirror [43]. The constant  $\alpha$  is determined by the Fresnel coefficient at the prism surface and by the angle of incidence onto the QWs. In our geometry  $\alpha = 0.43$ .

Figures 3(a)–3(c) show the local driving [31] MIR field  $E_{\text{lo}}(t)$  (dashed lines) and  $E_{\text{em}}(t)$  (solid lines) for MIR field amplitudes corresponding to pulse areas of approximately  $1\pi$ ,  $2\pi$ , and  $3\pi$ . The transients exhibit clear signatures of IS Rabi oscillations [23] as evident from the phase shifts between  $E_{\text{em}}(t)$  and  $E_{\text{lo}}(t)$  [Figs. 3(g)–3(i)]. For the  $1\pi$  pulse we find an essentially constant phase shift of  $\approx 1\pi$  corresponding to an absorptive IS response. For the  $2\pi$  pulse, the phase shift changes from  $\approx 1\pi$  to  $\approx 0$ , demonstrating a change from absorption to gain. For the  $3\pi$  pulse, the IS response becomes absorptive again, leading to two consecutive changes of the phase shift.

Time-domain results of the two-color 2D experiments are summarized in Fig. 4. In Figs. 4(a) and 4(c), the phase-resolved MIR and THz electric fields  $E_{\text{MIR+THz}}(t, \tau)$  transmitted through the sample are plotted as a function of real time  $t$  and delay  $\tau$  for two MIR amplitudes. The  $\tau$ -independent MIR field has vertical and the  $\tau$ -dependent THz field diagonal phase fronts. Figures 4(b) and 4(d) show the nonlinear signal  $E_{\text{NL}}(t, \tau) = E_{\text{MIR+THz}}(t, \tau) - E_{\text{MIR}}(t) - E_{\text{THz}}(t, \tau)$ , where  $E_{\text{MIR}}$  and  $E_{\text{THz}}$  are the transmitted fields when only one of the pulses (MIR or THz) interacts with the sample. This nonlinear signal represents the total nonlinear response up to arbitrary order in the incident fields. For a low MIR amplitude [Fig. 4(b)], the nonlinear signal occurs at negative values of  $\tau$  and mainly after the MIR pulse at long  $t$ , giving evidence of a perturbed free induction decay (PFID) [44]. At high MIR amplitudes [Fig. 4(d)], the signal is present only during the temporal pulse overlap.

To separate the different nonlinear contributions, we derive the frequency-domain signal  $E_{\text{NL}}(\nu_t, \nu_\tau)$  as a function of  $\nu_t$  and  $\nu_\tau$  by a two-dimensional Fourier transform [40,41]. As shown in Fig. 4(e), only a THz-pump–MIR-probe signal  $E_{\text{NL}}$  at the frequency position  $(\nu_t = \nu_0, \nu_\tau = 0)$  is present, while MIR-pump–THz-probe and four-wave-mixing signals are absent. For a higher signal-to-noise ratio,  $E_{\text{NL}}(\nu_t, \nu_\tau)$  is filtered to keep only the THz-pump–MIR-probe component and then back transformed to the time domain.

A representative PFID transient at  $\tau = 0$  measured at a low MIR field amplitude is shown in Fig. 2(e), demonstrating the slow IS polarization decay of  $T_{\text{decay}} = 0.63$  ps in our sample at low temperatures. By back transforming  $E_{\text{NL}}(\nu_t, \nu_\tau)$  only along  $\tau$  we obtain the spectrally resolved  $E_{\text{NL}}(\nu_t, \tau)$ . The quantity  $|E_{\text{NL}}(\nu_t, \tau)|^2$  corresponds to the spectrally resolved intensity radiated by the IS polarization for a delay  $\tau$  [dashed line in Fig. 2(d)]. For a small MIR amplitude, this quantity is independent of  $\tau$ . The line position agrees well with the IS absorption spectrum [solid line in Fig. 2(d)], but the linewidth is much narrower (0.5 THz) because of the better spectral resolution. We also derive the spectrally resolved pump-probe signals  $E_{\text{NL}}(\nu_t, \tau) \cdot E_{\text{MIR}}^*(\nu_t)$  for low and high MIR fields [Figs. 4(f) and 4(i)].  $E_{\text{MIR}}^*(\nu_t)$  is the complex conjugate of the MIR field in the frequency domain derived from the measured  $E_{\text{MIR}}(t)$ .

In Figs. 3(d)–3(f), the nonlinear signal  $E_{\text{NL}}(t, \tau)$  is plotted for fixed values of  $\tau$  and different MIR pulse areas. For a closer inspection, we show the THz-induced phase difference of the emitted field in Figs. 3(g)–3(i). This phase difference increases with  $t$  and—for the  $2\pi$  and  $3\pi$  MIR pulses—changes its sign whenever the Rabi oscillation switches from absorption to gain or vice versa. This shows that the THz pulse does not change the Rabi frequency but the phase of the emitted signal. Such phase changes also affect the frequency-resolved

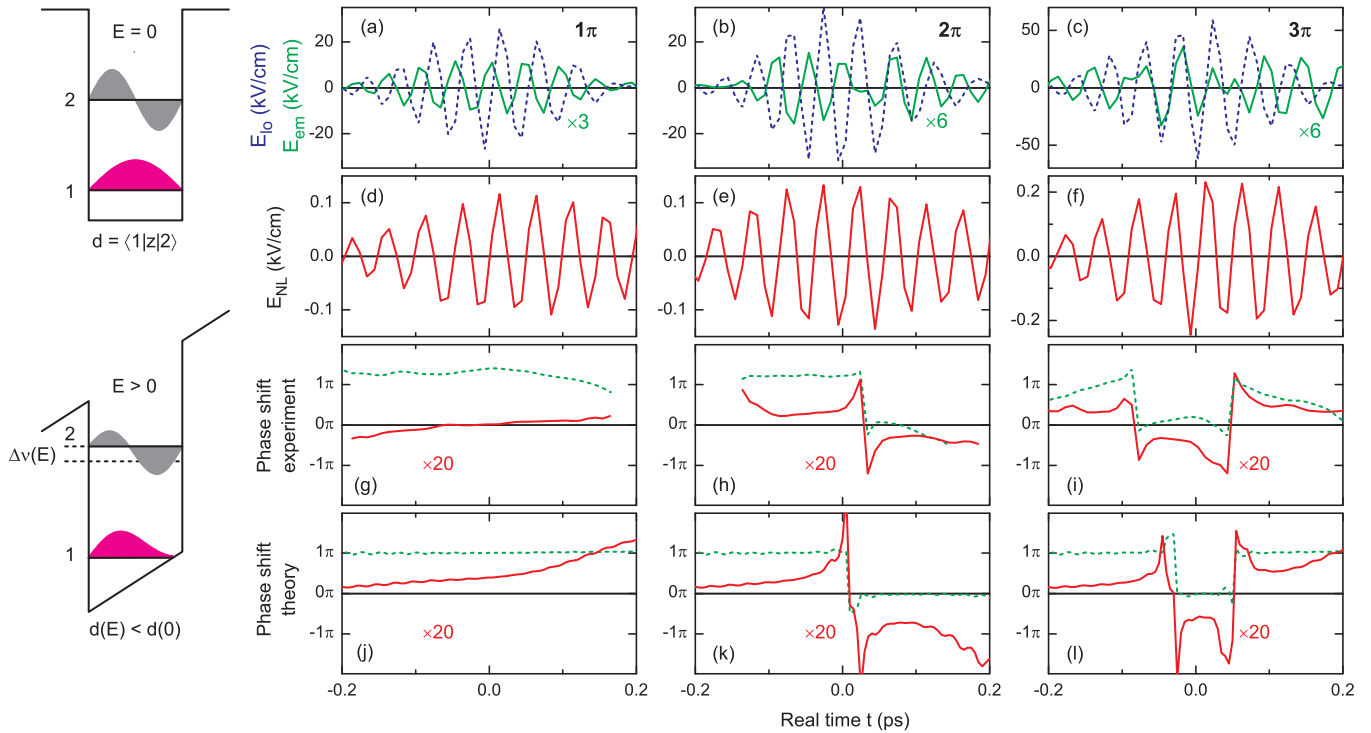


FIG. 3. (Color online) Left: Schematic of the potential and wave functions of the quantum well with (bottom) and without (top) applied THz field. For clarity, the electric field and the level shifts shown are much larger than in the actual experiment. (a)–(c) Emitted fields  $E_{em}(t)$  (green solid lines) from the  $1 \leftrightarrow 2$  IS transition and the corresponding MIR driving fields  $E_{10}(t)$  (blue dashed lines). (d)–(f) Nonlinear signal  $E_{NL}(t)$  induced by the THz field. (g)–(i) Green dashed line, phase shift between the emitted field  $E_{em}(t)$  and the driving field  $E_{10}(t)$ , showing Rabi oscillations. Red solid line, THz-induced change of the phase shift. (j)–(l) Calculated phase shifts. The left panels correspond to a pulse area of  $1\pi$  at  $\tau = -0.18$  ps, the middle panels to  $2\pi$  at  $\tau = -0.09$  ps, and the right panels to  $3\pi$  at  $\tau = -0.34$  ps.

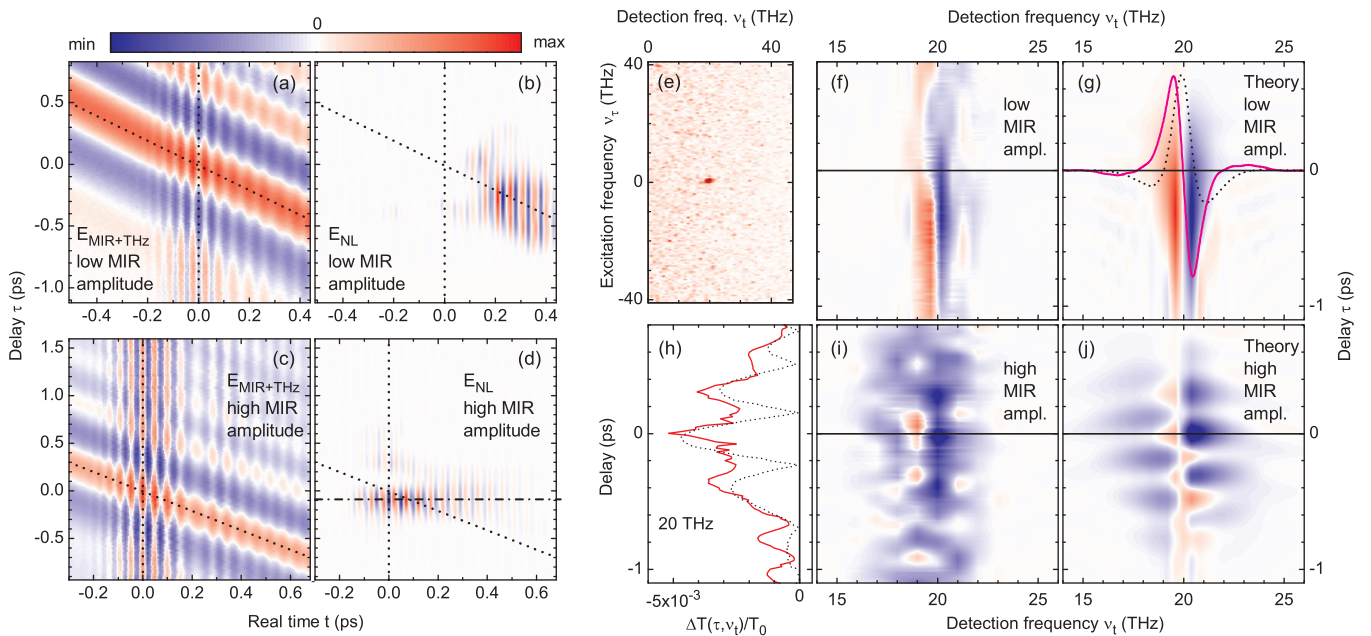


FIG. 4. (Color) (a),(c) Two-dimensional transients of resonant MIR and nonresonant THz electric fields transmitted through the sample, as a function of the real time  $t$  and the delay  $\tau$ . (b),(d) Corresponding nonlinear signal. The MIR field amplitude is 3 kV/cm, i.e., in the linear range, in (a) and (b) and 30 kV/cm (pulse area  $2\pi$ ) in (c) and (d). The dotted lines show the pulse centers; the dash-dotted line in (d) gives the position of the transient in Fig. 3(e). (e) Two-dimensional spectral density of the nonlinear signal as a function of the detection frequency  $\nu_t$  and the excitation frequency  $\nu_\tau$ . (f),(i) Measured spectrally resolved THz-pump-MIR-probe signal for low (f) and high [(i), pulse area  $2\pi$ ] MIR amplitude as a function of  $\nu_t$  and  $\tau$ . (g),(j) Calculated spectrally resolved pump-probe signals corresponding to the experiments shown in (f) and (i). (g) Solid line: dispersive signal at  $\tau = 0$ . Dashed line: symmetric signal at  $\tau = 0$  for a 20 THz pump–20 THz probe experiment in the  $\chi^{(3)}$  limit. (h) Solid line, cut through (i) at  $\nu_t = 20$  THz together with the magnitude of the THz electric field (dashed line, normalized).

pump-probe signals of Figs. 4(f) and 4(i). For low MIR fields, there is an increase of transmission below  $\nu_0$  and a decrease of transmission above, due to the THz-induced phase change [Fig. 3(g)]. For a pulse area of  $2\pi$  [Figs. 4(i) and 4(j)], the  $\tau$  dependence of the frequency-resolved pump-probe signal shows an oscillatory signature induced by the maxima of the instantaneous THz intensity.

### III. DISCUSSION

In this section, we discuss the physical mechanisms governing the observed linear and nonlinear IS response in presence of the nonresonant THz field. For a first qualitative insight into the general behavior, dynamical frequency shifts of a two-level system are considered in the Autler-Townes approach. Figure 1(b) shows a schematic sequence of a resonant MIR pulse and a THz half-cycle pulse delayed by 0.4 ps. Figure 1(c) shows the electric field transient emitted by the coherent polarization generated by the resonant MIR pulse in the regime of a linear MIR response. At exact resonance, the emitted field has a phase opposite to the driving field, corresponding to absorption. The amplitude of the emission decays exponentially with the dephasing time  $T_2$ . For a sufficiently long  $T_2$ , the delayed THz half cycle at  $t = 0.4$  ps causes a blueshift of the transition frequency resulting in a phase shift of the emitted field after the THz pulse [Fig. 1(c)]. It is important to note that the amplitude of the coherent polarization is not affected by the interaction with the off-resonant pulse, i.e., exclusively the phase of the optical excitation is manipulated but not the energy content in the quantum mechanical system. As will be discussed below, similar phase shifts are observed in the regime of a distinctly nonlinear IS response.

#### A. Influence of a THz field on intersubband Rabi oscillations

We now address the observed nonlinear IS response. The THz pulse generates an energy gradient along the  $z$  direction superimposed on the QW confinement potential (left of Fig. 3). For a field amplitude of 30 kV/cm and a QW width  $L = 11$  nm, the energy difference over  $L$  is 33 meV, corresponding to roughly 10% of the total electron confinement energy. In this new confinement potential, both the wave functions of the  $n = 1$  and  $n = 2$  subbands and the energy separation  $h\nu$  of the two subbands are modified. The reduced spatial overlap of the two wave functions leads to a reduction of the IS transition dipole moment from  $d_0 = e \times 2.5$  nm (derived from an eight-band  $\vec{k} \cdot \vec{p}$  calculation [45]) to  $d(E) \approx d_0[1 - 2(d_0E/h\nu_0)^2]$ , while the change in energy separation  $h\Delta\nu(E) \approx 2(d_0E)^2/h\nu_0$  blueshifts the frequency of the IS transition [46].

Because of the reduced IS dipole, one expects [46] an absorption decrease in the pump-probe experiments and—at high MIR fields—a reduced Rabi frequency. Such predictions are in sharp contrast to our data, clearly displaying an enhanced IS absorption [Figs. 2(a) and 4] and an unchanged Rabi frequency (Fig. 3). For a proper analysis, one has to take into account the influence of the detuning  $h\Delta\nu(E)$  on the Rabi frequency, i.e., one must consider the generalized Rabi frequency  $h\nu_{\text{Rabi}}(E) = \{[d(E)E]^2 + [h\Delta\nu(E)]^2\}^{1/2} \approx d_0[1 + 4(d_0E/h\nu_0)^4]E = d_{\text{eff}}(E)E$  [47]. Our experiments are

in the limit  $d_0E/h\nu_0 < 0.1$ , so that both the effective transition dipole moment  $d_{\text{eff}}(E) \approx d_0$  and the Rabi frequency  $\nu_{\text{Rabi}}$  remain essentially unchanged. We conclude that the field-induced changes of the IS transition frequency  $\Delta\nu(E)$  dominate the nonlinear response.

The THz-induced blueshift of the IS transition frequency results in a phase shift of  $E_{\text{em}}(t)$ , the emitted MIR field. These phase shifts are shown in Figs. 3(g)–3(i). For low enough MIR amplitude, i.e., outside the regime of Rabi oscillations [Fig. 3(g)], the phase shift increases with time, i.e., it adds up from cycle to cycle of  $E_{\text{em}}(t)$ , as expected for a blueshift of the frequency. For an analysis, we consider the IS transitions an ensemble of noninteracting two-level systems [48] and describe the light-matter interactions with the optical Bloch equations [23,49]. In solving Eq. (1) of [23], the total electric field, the sum of THz and MIR fields, is used. Since the frequencies of both fields are very different, both the slowly varying envelope and the rotating-wave approximations are not applicable, requiring a full solution of the Bloch equations.

Calculated phase shifts are shown in Figs. 3(j) to 3(l); they reproduce the experimental key features. Both in experiment and theory, the sign of the nonlinear phase changes exactly at the times at which absorption/gain switching occurs. The amplitudes of the calculated nonlinear phase shifts are somewhat larger than observed in the experiment [panels (g) to (i)]. The larger calculated phase shifts are probably caused by neglecting interactions with higher-lying QW levels which reduce the THz-induced phase shifts.

#### B. Spectrally resolved THz-pump–MIR-probe experiments

The spectrally resolved THz-pump–MIR-probe experiments give a clear signature of the THz-induced blueshift expected in the Autler-Townes picture [Fig. 1(a)]. In the time-integrated detection of a pump-probe signal, the field emitted by the sample's polarization [cf. Fig. 1(c)] interferes with the transmitted probe field on the detector. Calculated pump-probe transients are shown in Figs. 4(g) and 4(j) next to their experimental counterparts (f) and (i). The solid line in panel (g) reveals a dispersive, i.e., a spectrally asymmetric signal at delay times  $\tau \leq 0$  being a hallmark of the blue-shifted IS resonance. In contrast, a simulation of the fully resonant situation in a 20 THz pump–20 THz probe experiment at low MIR fields shows the well-known perturbed free induction decay at  $\tau \leq 0$ , with symmetric detuning oscillations around the IS absorption resonance and a bleach signal in the center (dashed line). A THz-MIR simulation with a  $2\pi$  MIR pulse [panel (j)] shows, similar to the experiment [panel (i)], a dispersive signal during the temporal overlap of THz and MIR pulses with pronounced maxima at the antinodes of the THz field.

A closer inspection of the solid line in Fig. 4(g) shows that the spectrally asymmetric signal at  $\tau = 0$  is not completely symmetric, so that the area under the positive signal (bleaching) is smaller than the area under the negative signal (induced absorption). This difference causes the THz-induced absorption observed in the spectrally integrated THz pump–MIR probe experiments [Fig. 2(a)] and will be discussed in the next section. Interestingly, the perturbed free induction decay extends to negative delay times of  $\approx -1$  ps. The spectrally asymmetric signal at  $\tau < -0.5$  ps is symmetric, corresponding

to a vanishing spectrally integrated absorption. In this range the THz pulse does not change the energy content in the system, as expected for an off-resonant pulse.

### C. THz-induced intersubband absorption

Finally, we identify the origin of the THz-induced IS absorption observed in the spectrally integrated THz-pump-MIR-probe experiments [Fig. 2(a)]. Such a nonlinear absorption during the pulse overlap is expected in the limit of strong radiative coupling, in which the IS linewidth is dominated by radiative damping rather than dephasing of the IS polarization. Radiative coupling and damping phenomena occurring in our sample geometry have been discussed in detail in Ref. [24] (Fig. 3 of this reference).

The linear IS absorption spectrum does not allow to distinguish the following two scenarios: (i) an IS absorption linewidth dominated by radiative damping together with a long  $T_2$  and (ii) IS absorption in the limit of weak radiative damping with a linewidth determined by the dephasing time  $T_2$ . In contrast, nonlinear spectroscopy including the present experiment can distinguish the two cases.

To clarify this issue, we consider the time-dependent energy absorbed in the sample given by  $I_{\text{abs}}(t) = \epsilon_0 c [E_{\text{tr}}^{\text{no}}(t)^2 - E_{\text{tr}}^{\text{gold}}(t)^2] = -\alpha^{-1} \epsilon_0 c E_{\text{em}}(t) E_{\text{lo}}(t)$  [50]. The time integral  $W_{\text{abs}}(t) = \int_{-\infty}^t I_{\text{abs}}(s) ds$  gives the amount of energy cumulatively transferred to the sample up to the time  $t$ , with the total (irreversible) absorption given by  $W_{\text{abs}}(\infty)$ . In Figs. 5 and 6 we show model calculations for low MIR fields for the two cases. To increase the visibility of the effects, the THz field amplitude in these calculations was chosen much higher than in the experiments.

For strong radiative damping (Fig. 5), panel (a) shows the local field acting on the IS dipoles  $E_{\text{lo}}^0(t)$  without THz excitation. At early times,  $E_{\text{lo}}^0(t)$  is dominated by the incident MIR field  $E_{\text{in}}(t)$ , and at late times by the emitted electric field from the IS polarization  $E_{\text{em}}^0(t)$ . The corresponding time-dependent absorption  $I_{\text{abs}}(t)$  is shown in Fig. 5(b). In the first part of the field transient  $E_{\text{lo}}^0(t)$ , a large amount of energy is stored in the system, while a significant fraction is reemitted at later times. As a consequence, the total absorbed MIR energy  $W_{\text{abs}}(\infty)$  is distinctly less than the maximal energy stored at early times. For comparison, panel (c) also shows the modulus of the IS polarization  $|P(t)|$ , demonstrating clearly the radiative character of the energy loss during the second part of  $E_{\text{lo}}^0(t)$ .

Next, we apply additionally a Gaussian THz half cycle pulse  $E_{\text{THz}}(t)$  [Fig. 5(a)] in temporal overlap with the MIR pulse, i.e., at  $\tau = 0$ . The THz pulse modifies both  $E_{\text{em}}(t)$  and  $E_{\text{lo}}(t)$  compared to the situation without THz excitation. The THz-induced phase shift of  $E_{\text{em}}(t)$  reduces the energy exchange  $I_{\text{abs}}(t)$  compared to that without THz excitation [Fig. 5(b)]. Since the phase shift is fully developed only after the end of the THz pulse, the energy irreversibly deposited in the sample  $W_{\text{abs}}(\infty)$  is larger with THz excitation. Thus the enhanced absorption found in the spectrally integrated THz-pump-MIR-probe experiments is a hallmark of radiative coupling in the QW sample.

For comparison, we calculated the response in the limit of weak radiative coupling (Fig. 6). In this case, THz excitation

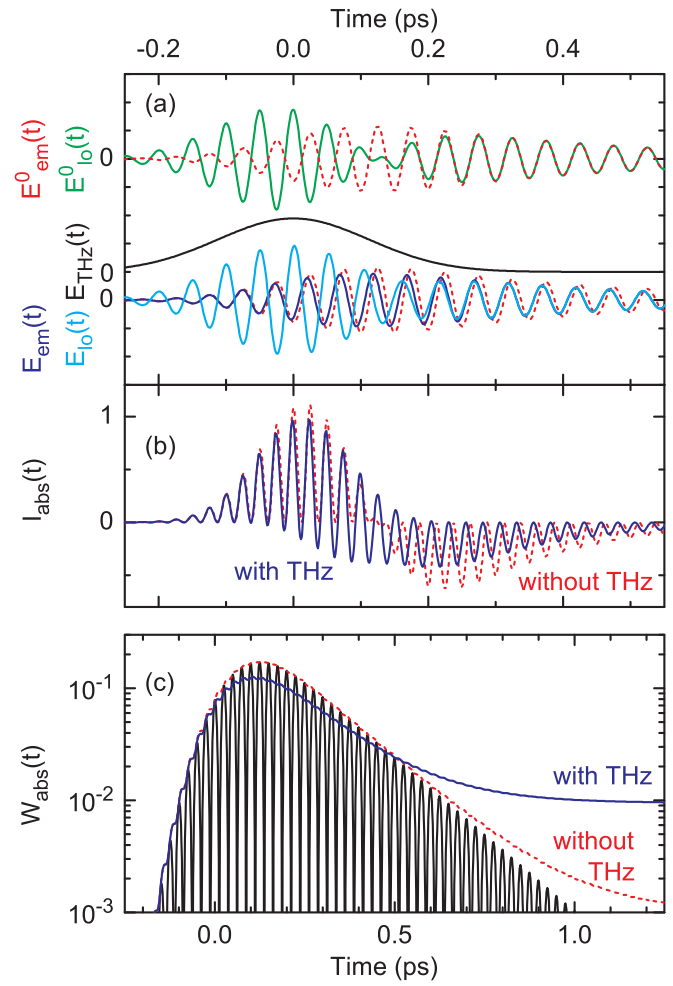


FIG. 5. (Color online) Model calculations for the THz-induced intersubband absorption during the temporal overlap of THz and MIR pulses, i.e., at  $\tau = 0$ . (a) Local field acting on the IS dipoles and field emitted by the intersubband polarization with [ $E_{\text{lo}}(t)$  and  $E_{\text{em}}(t)$ ] and without [ $E_{\text{lo}}^0(t)$  and  $E_{\text{em}}^0(t)$ ] a Gaussian THz half cycle pulse with the electric field transient  $E_{\text{THz}}(t)$ . (b) Time-dependent energy absorption of the sample  $I_{\text{abs}}(t)$  with (blue solid line) and without (red dashed line) THz excitation. (c) Energy deposited in the sample  $W_{\text{abs}}(t)$  for the two cases. The black curve shows for comparison the modulus of the IS polarization  $|P(t)|$ .

leads to a reduction of absorbed energy [panel (c)], as the THz field affects the polarization phase in the absorptive region at early times. This is in sharp contrast to the experimental observation in Fig. 2(a).

Finally, we estimate the radiative damping rate of our sample and compare it with the experimentally observed total decay rate  $\gamma_{\text{tot}} = (0.63 \text{ ps})^{-1}$  of the coherent polarization shown in Fig. 2(e). The radiative damping rate can be easily estimated with the formalism developed in Ref. [43]. For our sample geometry we find a radiative damping rate of  $\gamma_{\text{rad}} = (0.9 \text{ ps})^{-1}$ , which definitely dominates the total polarization decay experimentally observed in Fig. 2(e). As a result we expect THz-induced absorption of resonant MIR radiation during the pulse overlap as observed in our experiment, shown in Fig. 2(a).

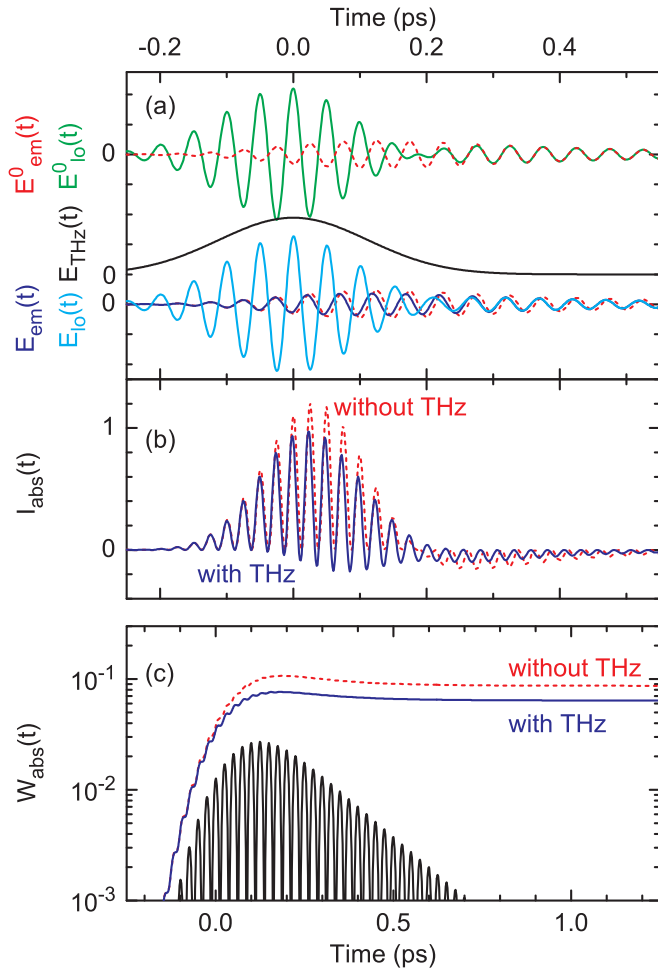


FIG. 6. (Color online) Model calculations for the THz-induced intersubband absorption in the weak radiative coupling limit. The plots have the same meaning as in Fig. 5.

#### IV. CONCLUSIONS AND OUTLOOK

In conclusion, we have demonstrated a scheme of nonresonant coherent control and analyzed the underlying light-matter interactions in detail. As a model case, linear and nonlinear intersubband excitations in  $n$ -doped semiconductor quantum wells were manipulated by a nonresonant THz field. The system's response was mapped in amplitude and phase by two-color two-dimensional THz-MIR spectroscopy. Our results demonstrate that a THz-induced frequency shift of the MIR intersubband transition is the predominant optical nonlinearity, giving rise to pronounced accumulated phase shifts in the emitted MIR electric field. This allows for control over the character of the overall response, i.e., a switching from a predominantly absorptive to emissive behavior by long THz transients of sufficient electric field amplitude. In

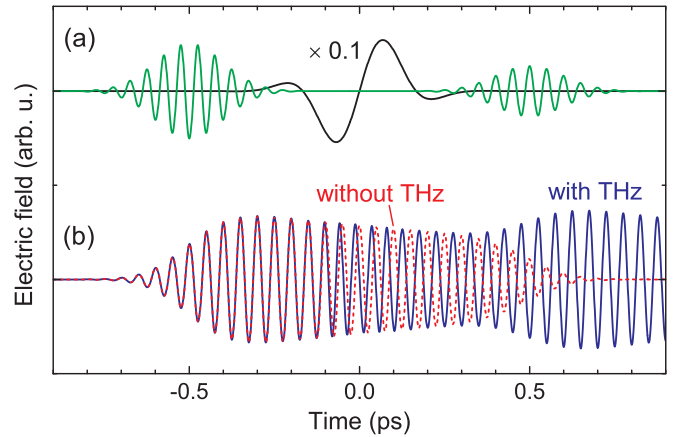


FIG. 7. (Color online) (a) Extended coherent control scheme using two resonant MIR (green) pulses and one off-resonant (black) THz pulse. (b) Red dashed line, MIR transient reemitted by the coherent IS polarization excited by the two phase-locked MIR pulses. The amplitude and phase of the second pulse at  $t = +0.5$  ps was chosen to completely remove the coherent excitation created by the first pulse at  $t = -0.5$  ps. Blue solid line, the off-resonant THz pulse around  $t = 0$  leads to a phase shift of the IS polarization, resulting in an increase of the IS emission by the second pulse.

contrast to resonant control schemes, the nonresonant THz field is—apart from minor propagation effects—not altered in the process of control. We envisage applications of this scheme in optoelectronic switching and an extension of the basic concept to other systems.

As an outlook, Fig. 7 presents the behavior calculated for an off-resonant control scheme based on two resonant MIR pulses and an off-resonant THz pulse. Without the THz pulse, one observes a MIR transient reemitted by the coherent IS polarization. For a proper choice of the amplitude and phase of the second pulse at  $t = +0.5$  ps it can completely remove the coherent excitation created by the first pulse at  $t = -0.5$  ps. Applying additionally the off-resonant THz pulse around  $t = 0$  changes the phase of the coherent emission generated by the first MIR pulse and results in an enhanced coherent IS emission after the second MIR pulse. Thus the off-resonant THz field controls the direction of the energy transfer between the second MIR pulse and the coherent IS excitation. An interesting aspect of this type of switching scheme is that there is no irreversible energy transfer between the off-resonant THz pulse and the quantum mechanical two-level system, i.e., the coherent IS excitation is switched in a “lossless” way.

#### ACKNOWLEDGMENT

We acknowledge financial support by the Deutsche Forschungsgemeinschaft: RE 806/9-1.

- [1] W. S. Warren, H. Rabitz, and M. Dahleh, *Science* **259**, 1581 (1993).
- [2] A. M. Weiner, *Rev. Sci. Instrum.* **71**, 1929 (2000).
- [3] P. C. M. Planken, I. Brener, M. C. Nuss, M. S. C. Luo, and S. L. Chuang, *Phys. Rev. B* **48**, 4903 (1993).

- [4] A. P. Heberle, J. J. Baumberg, and K. Köhler, *Phys. Rev. Lett.* **75**, 2598 (1995).
- [5] M. Woerner and J. Shah, *Phys. Rev. Lett.* **81**, 4208 (1998).
- [6] R. Atanasov, A. Haché, J. L. P. Hughes, H. M. van Driel, and J. E. Sipe, *Phys. Rev. Lett.* **76**, 1703 (1996).

- [7] M. Aeschlimann, M. Bauer, D. Bayer, T. Brixner, F. J. García de Abajo, W. Pfeiffer, M. Rohmer, C. Spindler, and F. Steeb, *Nature (London)* **446**, 301 (2007).
- [8] T. Feurer, J. C. Vaughan, and K. A. Nelson, *Science* **299**, 374 (2003).
- [9] M. J. J. Vrakking and S. Stolte, *Chem. Phys. Lett.* **271**, 209 (1997).
- [10] A. Assion, T. Baumert, M. Bergt, T. Brixner, B. Kiefer, V. Seyfried, M. Strehle, and G. Gerber, *Science* **282**, 919 (1998).
- [11] P. Nuernberger, G. Vogt, T. Brixner, and G. Gerber, *Phys. Chem. Chem. Phys.* **9**, 2470 (2007).
- [12] V. I. Prokhorenko, A. M. Nagy, S. A. Waschuk, L. S. Brown, R. R. Birge, and R. J. D. Miller, *Science* **313**, 1257 (2006).
- [13] B. J. Pearson, J. L. White, T. C. Weinacht, and P. H. Bucksbaum, *Phys. Rev. A* **63**, 063412 (2001).
- [14] K. Bergmann, H. Theuer, and B. W. Shore, *Rev. Mod. Phys.* **70**, 1003 (1998).
- [15] N. V. Vitanov, T. Halfmann, B. W. Shore, and K. Bergmann, *Annu. Rev. Phys. Chem.* **52**, 763 (2001).
- [16] M. Wagner, H. Schneider, D. Stehr, S. Winnerl, A. M. Andrews, S. Scharfner, G. Strasser, and M. Helm, *Phys. Rev. Lett.* **105**, 167401 (2010).
- [17] S. H. Autler and C. H. Townes, *Phys. Rev.* **100**, 703 (1955).
- [18] A. M. Bonch-Bruевич and V. A. Khodovoi, *Usp. Fiz. Nauk* **93**, 71 (1967) [*Sov. Phys. Usp.* **10**, 637 (1968)].
- [19] M. Helm, in *Intersubband Transitions in Quantum Wells: Physics and Device Applications I*, edited by H. C. Liu and F. Capasso (Academic Press, New York, 2000), pp. 1–100.
- [20] A. Delteil, A. Vasanelli, Y. Todorov, C. Feuillet Palma, M. Renaudat St-Jean, G. Beaudoin, I. Sagnes, and C. Sirtori, *Phys. Rev. Lett.* **109**, 246808 (2012).
- [21] M. Wagner, M. Helm, M. S. Sherwin, and D. Stehr, *Appl. Phys. Lett.* **99**, 131109 (2011).
- [22] D. Dietze, J. Darmo, and K. Unterrainer, *Opt. Express* **20**, 23053 (2012).
- [23] C. W. Luo, K. Reimann, M. Woerner, T. Elsaesser, R. Hey, and K. H. Ploog, *Phys. Rev. Lett.* **92**, 047402 (2004).
- [24] T. Shih, K. Reimann, M. Woerner, T. Elsaesser, I. Waldmüller, A. Knorr, R. Hey, and K. H. Ploog, *Phys. Rev. B* **72**, 195338 (2005).
- [25] J. Faist, F. Capasso, D. L. Sivco, A. L. Hutchinson, C. Sirtori, and A. Y. Cho, *Science* **264**, 553 (1994).
- [26] R. Köhler, A. Tredicucci, F. Beltram, H. E. Beere, E. H. Linfield, A. G. Davies, D. A. Ritchie, R. C. Iotti, and F. Rossi, *Nature (London)* **417**, 156 (2002).
- [27] C. Sirtori, S. Dhillon, C. Faugeras, A. Vasanelli, and X. Marcadet, *Phys. Status Solidi A* **203**, 3533 (2006).
- [28] F. R. Giorgetta, E. Baumann, M. Graf, Q. Y. C. Manz, K. Kohler, H. E. Beere, D. A. Ritchie, E. Linfield, A. G. Davies, Y. Fedoryshyn, H. Jackel, M. Fischer, J. Faist, and D. Hofstetter, *IEEE J. Quantum Electron.* **45**, 1039 (2009).
- [29] R. A. Kaindl, K. Reimann, M. Woerner, T. Elsaesser, R. Hey, and K. H. Ploog, *Phys. Rev. B* **63**, 161308(R) (2001).
- [30] I. I. Rabi, *Phys. Rev.* **51**, 652 (1937).
- [31] T. Stroucken, A. Knorr, P. Thomas, and S. W. Koch, *Phys. Rev. B* **53**, 2026 (1996).
- [32] F. Eickemeyer, R. A. Kaindl, M. Woerner, T. Elsaesser, S. Barbieri, P. Kruck, C. Sirtori, and J. Nagle, *Appl. Phys. Lett.* **76**, 3254 (2000).
- [33] F. Eickemeyer, M. Woerner, A. M. Weiner, T. Elsaesser, R. Hey, and K. H. Ploog, *Appl. Phys. Lett.* **79**, 165 (2001).
- [34] M. Born and E. Wolf, *Principles of Optics*, 7th ed. (Cambridge University Press, Cambridge, UK, 1999).
- [35] The long-lived signal is caused by the generation of electron-hole pairs in the substrate by the intense THz pulse [36] and the subsequent change of absorption and reflection. The time constant of this signal is given by the carrier recombination time, which is in the ns range [37].
- [36] W. Kuehn, P. Gaal, K. Reimann, M. Woerner, T. Elsaesser, and R. Hey, *Phys. Rev. B* **82**, 075204 (2010).
- [37] P. D. Dapkus, N. Holonyak, Jr., R. D. Burnham, D. L. Keune, J. W. Burd, K. L. Lawley, and R. E. Walline, *J. Appl. Phys.* **41**, 4194 (1970).
- [38] Q. Wu and X.-C. Zhang, *Appl. Phys. Lett.* **67**, 3523 (1995).
- [39] Q. Wu and X.-C. Zhang, *Appl. Phys. Lett.* **71**, 1285 (1997).
- [40] W. Kuehn, K. Reimann, M. Woerner, and T. Elsaesser, *J. Chem. Phys.* **130**, 164503 (2009).
- [41] W. Kuehn, K. Reimann, M. Woerner, T. Elsaesser, and R. Hey, *J. Phys. Chem. B* **115**, 5448 (2011).
- [42] Here we have the sum and not the difference, since the total reflection leads to a sign change of the transmitted field. In the following  $E_{tr}(t)$  without a superscript will denote  $E_{tr}^{\text{gold}}(t)$ .
- [43] I. Waldmüller, J. Förstner, S. C. Lee, A. Knorr, M. Woerner, K. Reimann, R. A. Kaindl, T. Elsaesser, R. Hey, and K. H. Ploog, *Phys. Rev. B* **69**, 205307 (2004).
- [44] M. Chachisvilis, H. Fidler, and V. Sundström, *Chem. Phys. Lett.* **234**, 141 (1995).
- [45] R. Eppenga, M. F. H. Schuurmans, and S. Colak, *Phys. Rev. B* **36**, 1554 (1987).
- [46] E. Ozturk, *Opt. Commun.* **332**, 136 (2014).
- [47] R. Loudon, *The Quantum Theory of Light* (Clarendon Press, Oxford, 1973).
- [48] I. Waldmueller, W. W. Chow, and A. Knorr, *Phys. Rev. B* **73**, 035433 (2006).
- [49] F. Bloch, *Phys. Rev.* **70**, 460 (1946).
- [50] P. Gaal, W. Kuehn, K. Reimann, M. Woerner, T. Elsaesser, R. Hey, J. S. Lee, and U. Schade, *Phys. Rev. B* **77**, 235204 (2008).